Supporting Information

Enhancing High-Performance Supercapattery Electrodes: Harnessing Structural and Compositional Synergies via Phosphorus Doping on Bimetallic Boride for Rapid Charging

Amarnath T. Sivagurunathan[a], T. Kavinkumar[a], Selvaraj Seenivasan[a], Yongchai Kwon[b,], and Do-Heyoung Kim[a,*]*

[a] School of Chemical Engineering, Chonnam National University, 77 Yongbong-ro, Gwangju 61186, Republic of Korea.

[b] Department of Chemical and Biomolecular Engineering, Seoul National University of Science and Technology, 232 Gongneung-ro, Nowon-gu, Seoul 01811, Republic of Korea.

*Corresponding author's email: kdhh@chonnam.ac.kr (D.-H. Kim), kwony@seoultech.ac.kr (Y. Kwon)

Tel. (office): +82-62-530-1894 (D.-H. Kim), +82-2-970-6805 (Y. Kwon)

Characterizations

X-ray diffraction (XRD) analysis was conducted using a Rigaku X-ray diffractometer with CuKα radiation. The morphology and microstructure of the samples were examined using high-resolution scanning electron microscopy (HR-SEM; JEOL JSM-7500F) and transmission electron microscopy (TEM; TECNAI G2 F20 TEM system). X-ray photoelectron spectroscopy (XPS) was employed using an ESCALAB-MKII system (VG Scientific Co.). XPS had an Al K alpha source, and the results had been characterized by the Fityk software. Gaussian as a fitting function was used to characterize the XPS results. Brunauer-Emmett-Teller (BET, ASAP2010, Micromeritics) analysis was used to determine the surface area of the prepared samples.

Supercapattery measurements

The electrochemical capacitive properties of the as-synthesized nanostructure electrodes were investigated in an aqueous 2 M KOH solution using a three-electrode cell. The as-fabricated materials on Ni foam, platinum (Pt) foil and standard calomel electrode (SCE) were employed as the working, counter, and reference electrodes, respectively. The mass loadings of P-NCB and R-GO were calculated to be 3.5 mg cm^{-2} and 2 mg cm^{-2} respectively. In the supercapattery cell, the P-NCB electrode was used as the positrode and R-GO as the negatrode with 2M KOH/PVA gel employed as the electrolyte.

The specific capacitance (C_s, F g^{-1}) and specific capacity (C_m, C g^{-1}) were calculated from galvanostatic charge/discharge (GCD) testing using the Eq. (1) and (2), respectively[1]:

$$C_s = \frac{2i/V\,dt}{m\,(V_f - V_i)^2} \qquad (1)$$

$$C_m = C_s \times \Delta V \quad (2)$$

where, m (g), i (A), (V_f-V_i), and $\int V\,dt$ are the mass of the active materials coated on the Ni foam, the applied current, the functional potential frame, and the integral area of the discharge curve, respectively.

The energy density (E) and power density (P) of the supercapattery were calculated according to Eq. (3) and (4), respectively:

$$E = \frac{I \int V\,dt}{3.6} \quad (3)$$

$$P = \frac{3600 \times E}{t} \quad (4)$$

where I (A g^{-1}) and t (s) are the current density, and discharge time of the supercapattery cell, respectively.

Supercapattery device fabrication

The solid-state supercapattery device was assembled by using optimized P-NCB as the positrode and R-GO as the negatrode with cellulose paper as a separator, respectively. A PVA–KOH gel electrolyte was used as the conducting medium in the assembled two-electrode device system. The gel electrolyte was prepared by taking about 10 gm PVA in 80 mL deionized water and kept at 160 °C for about 4 h for complete dissolution. Separately, 2M KOH solution was prepared in 20 mL deionized water and added to the above solution to form a PVA–KOH gel electrolyte with required consistency. Both the negatrode and positrodes were soaked in the electrolyte along with the cellulose paper for about 5 min. After proper soaking, the device was assembled and allowed

to dry under the air atmosphere for about 24 h to obtain a completely solidified device. The dried solid-state supercapattery device was subjected to cyclic voltammetry and galvanostatic charge–discharge analysis. The cyclic stability of the fabricated asymmetric supercapacitor device has been recorded using an automatic battery cycler (WBCS3000)[2].

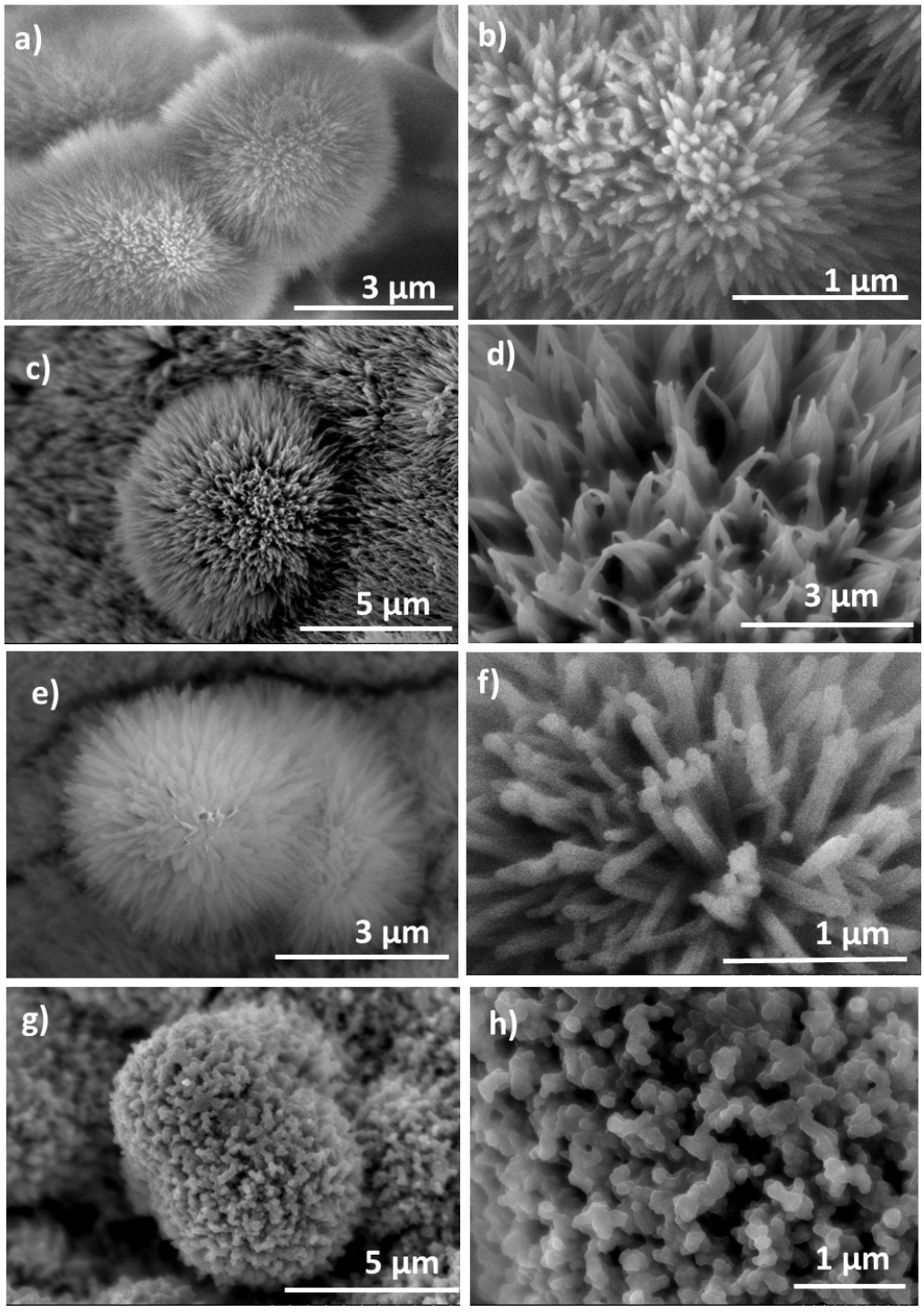

Fig. S1. SEM images of the nanostructure of the (a, b) NC, (c, d) NCB, (e, f) P-NC and (g, h) P-NCB samples.

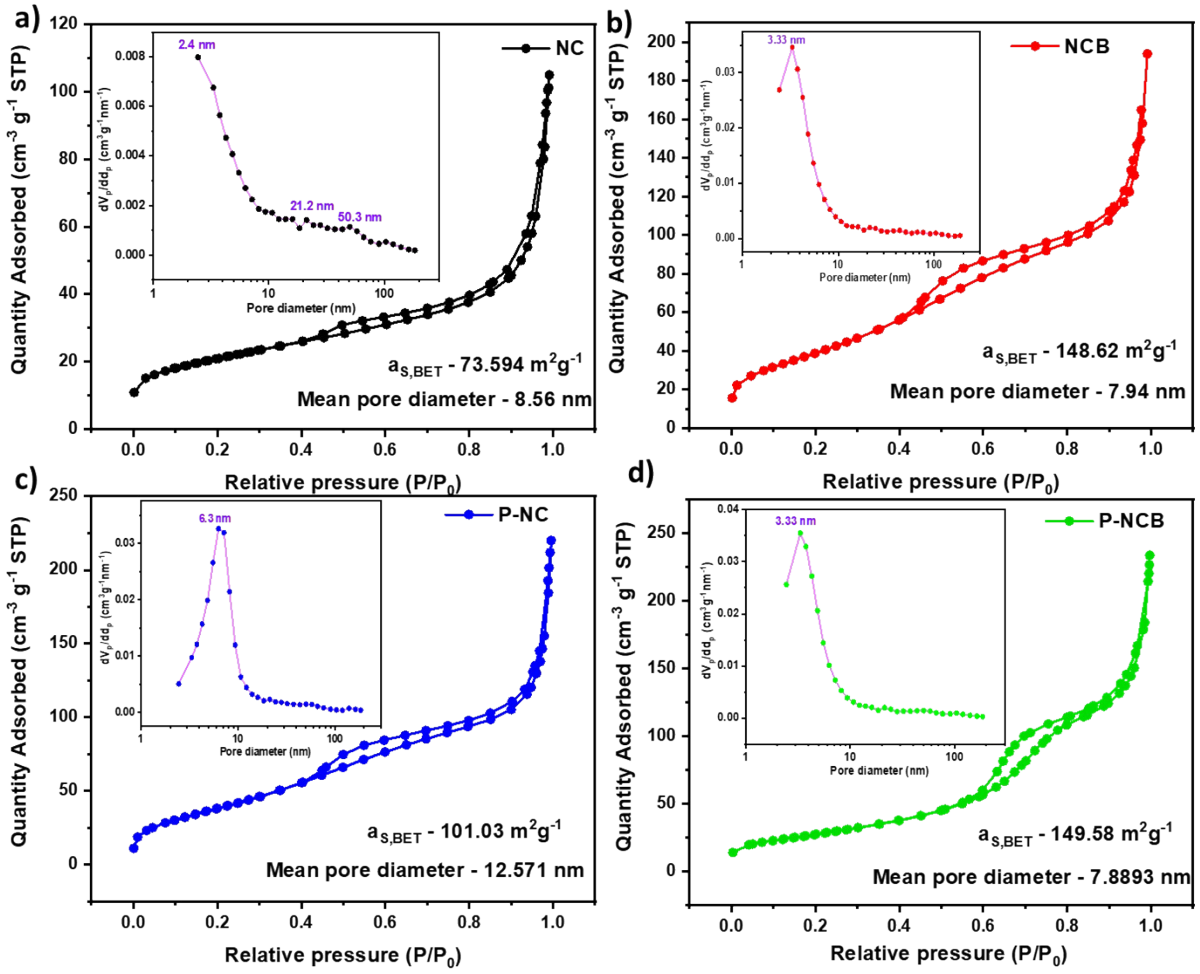

69

70 **Fig. S2.** N_2 adsorption–desorption isotherms for (a) NC, (b) NCB, (c) P-NC and (d) P-NCB

71 samples. The inset shows the corresponding pore size distribution profiles.

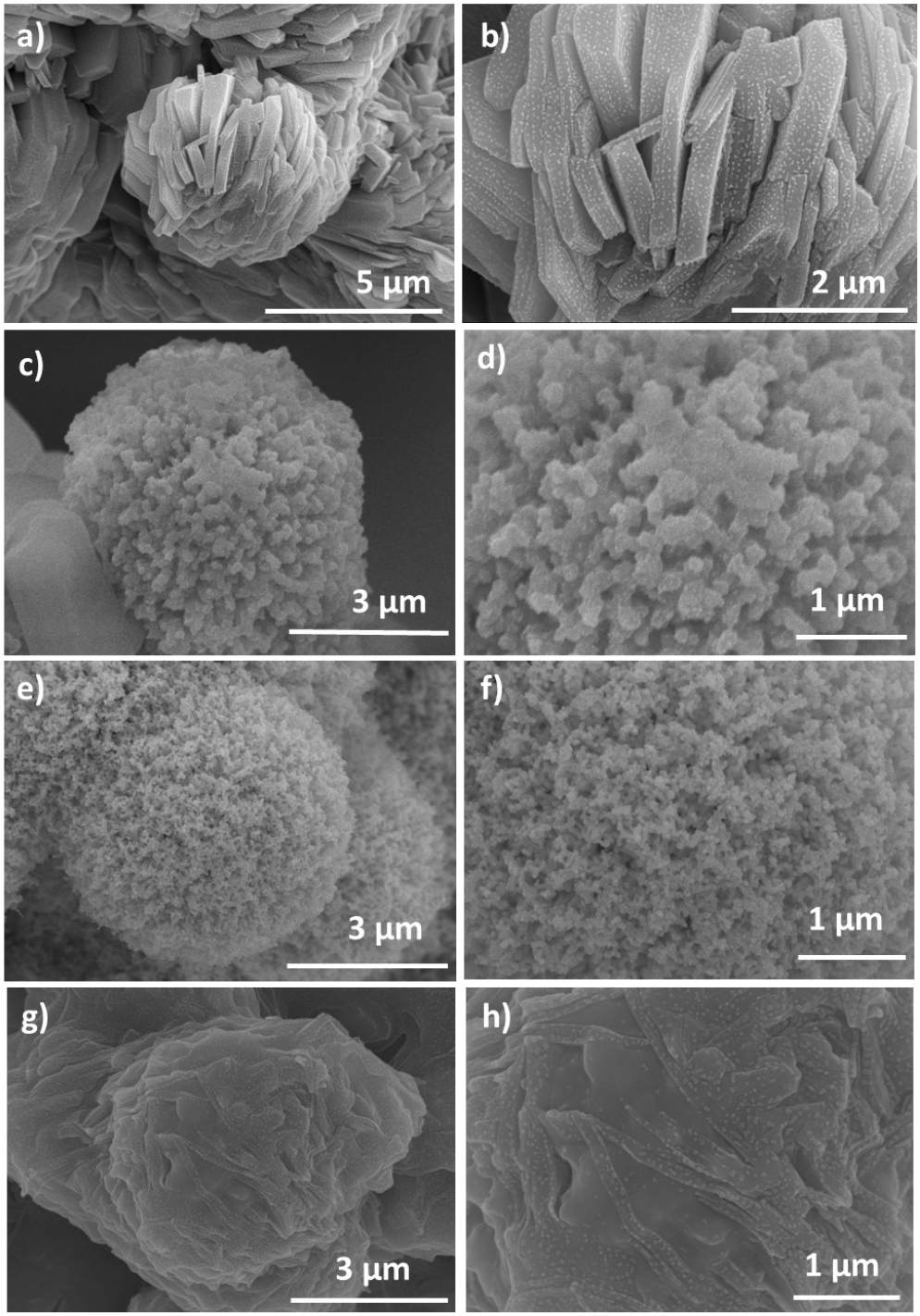

Fig. S3. SEM images of the nanostructure of the (a, b) P-NCB-70-350°, (c, d) P-NCB-210-350°, (e, f) P-NCB-140-300° and (g, h) P-NCB-140-400° samples.

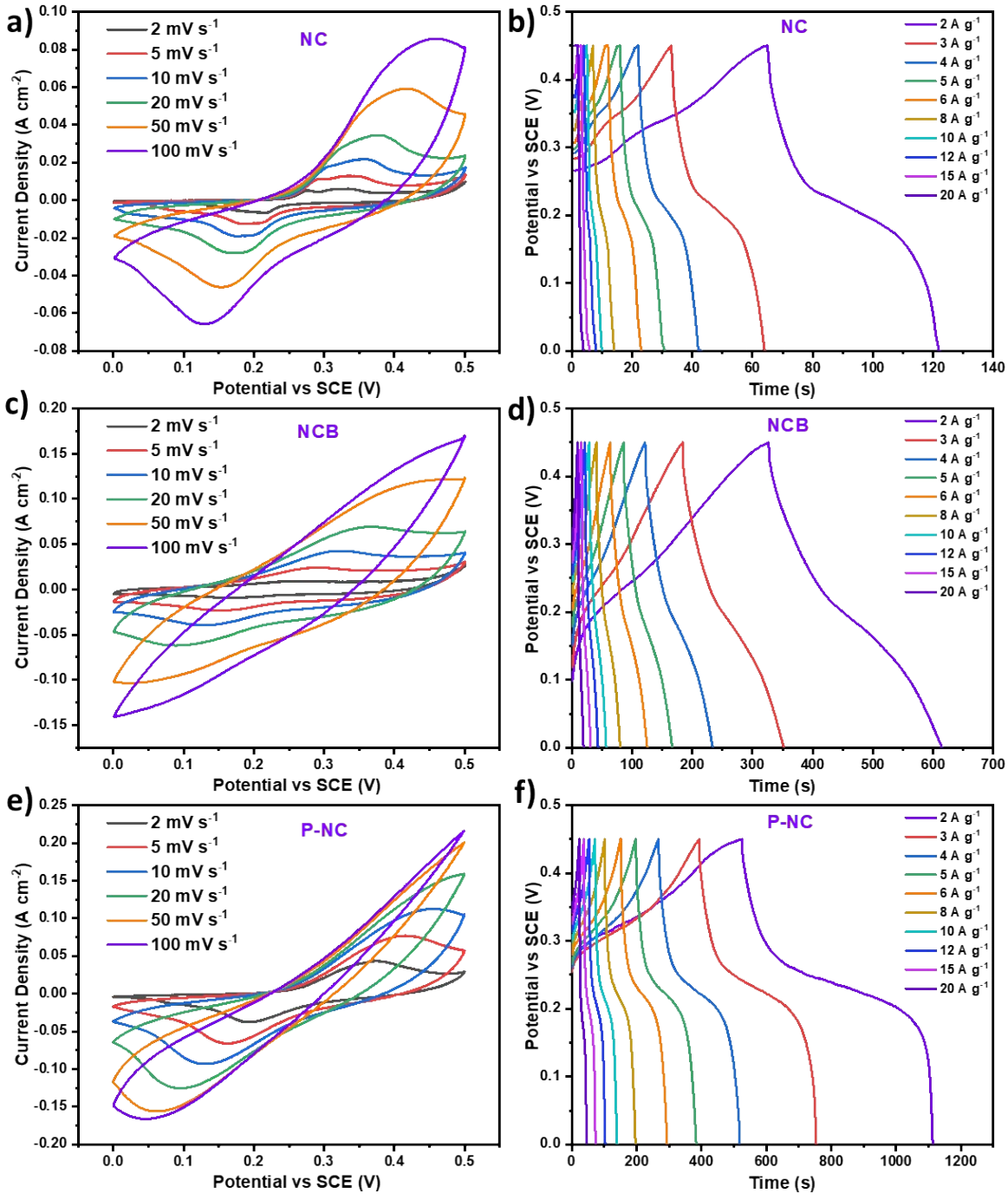

Fig. S4. CV profile at different scan rate and GCD profile at different current density of (a, b) NC, (c, d) NCB and (e, f) P-NC samples respectively.

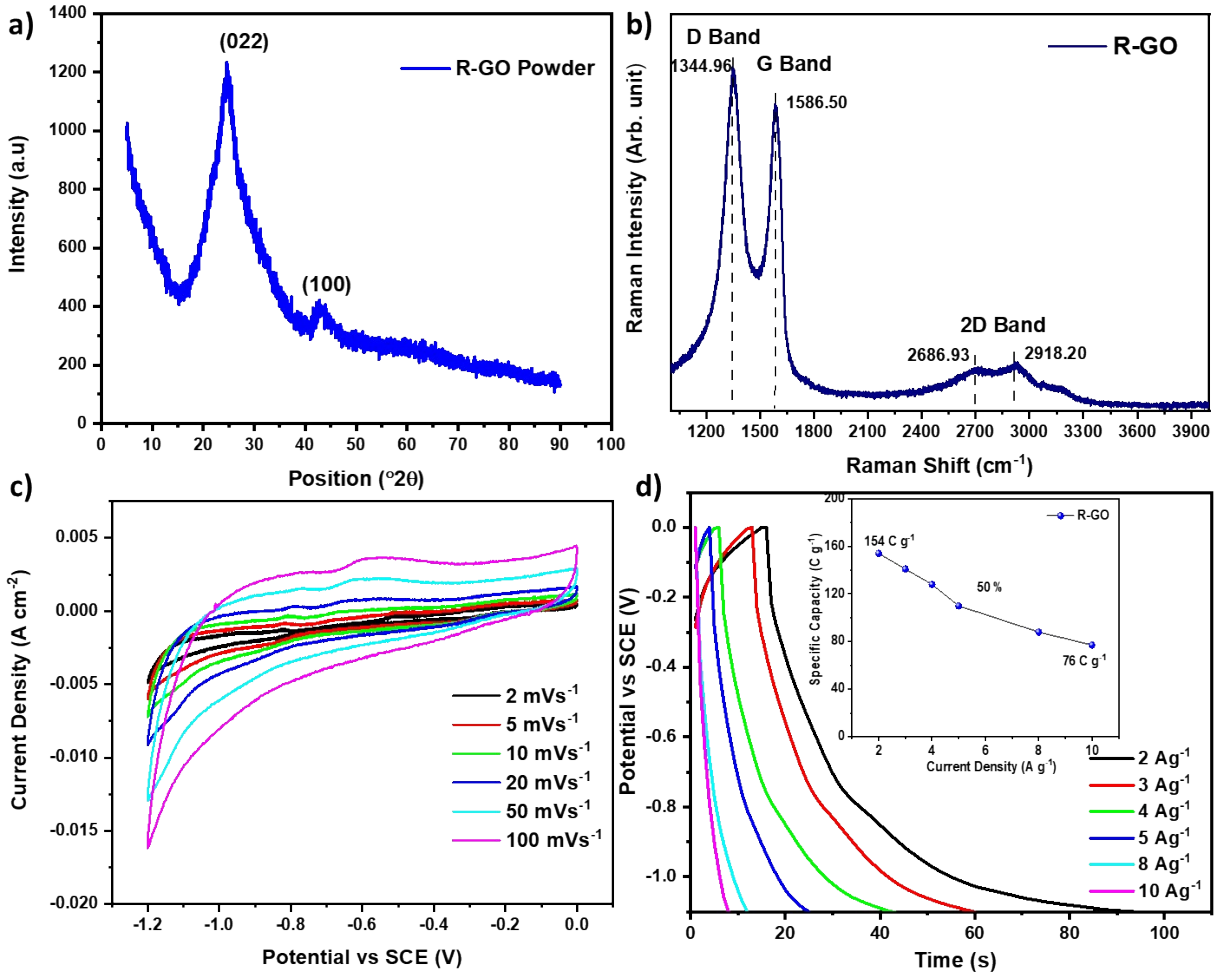

79

80 **Fig. S5.** R-GO characterizations (a) XRD spectra, (b) Raman Spectra, (c) CV profile at different

81 scan rate, (d) GCD profile at different current density.

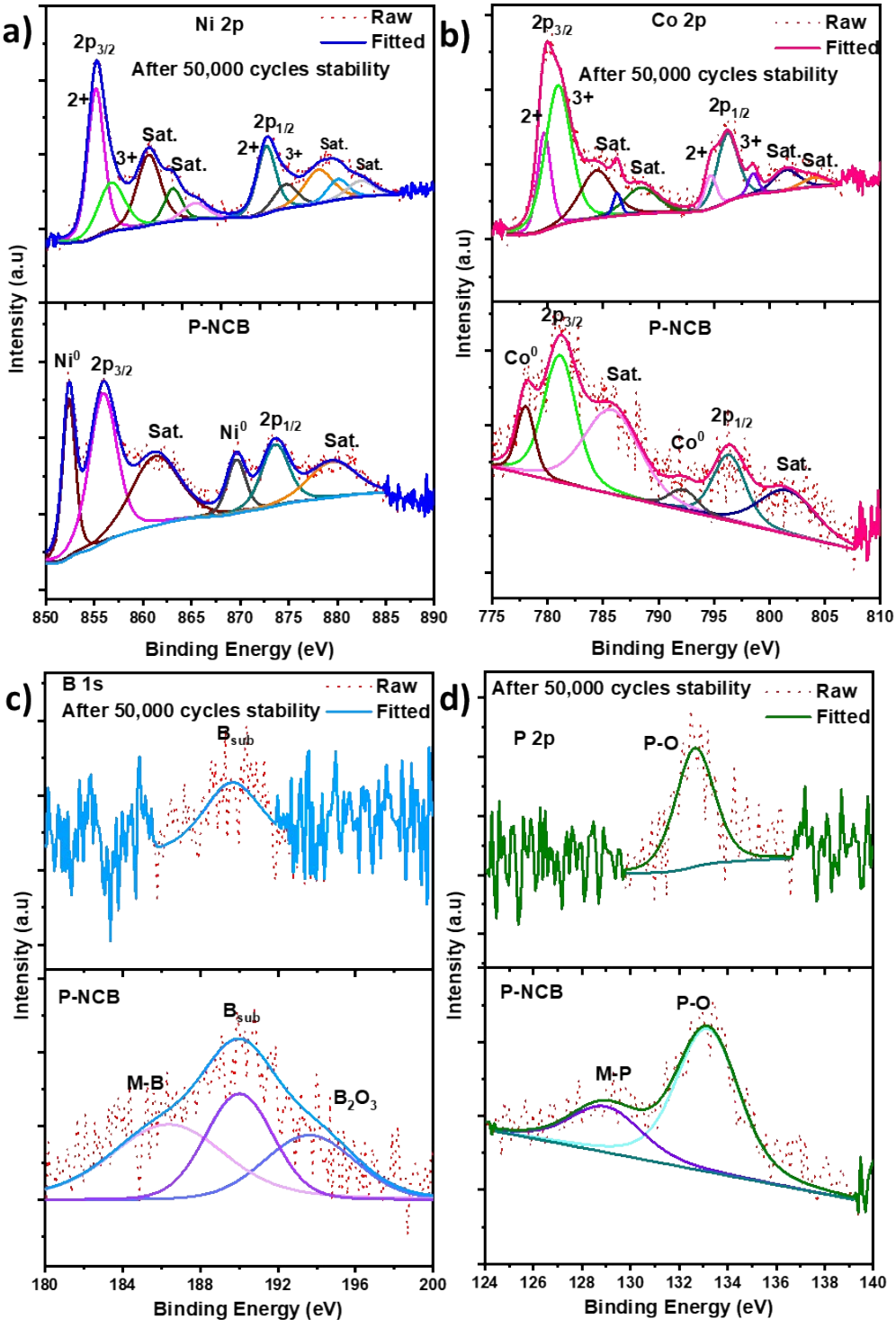

82

83 **Fig. S6.** XPS spectra of post 50,000 cycles of GCD stability of P-NCB sample (a) Ni 2p, (b) Co

84 2p, (c) B 1s and (d) P 2p.

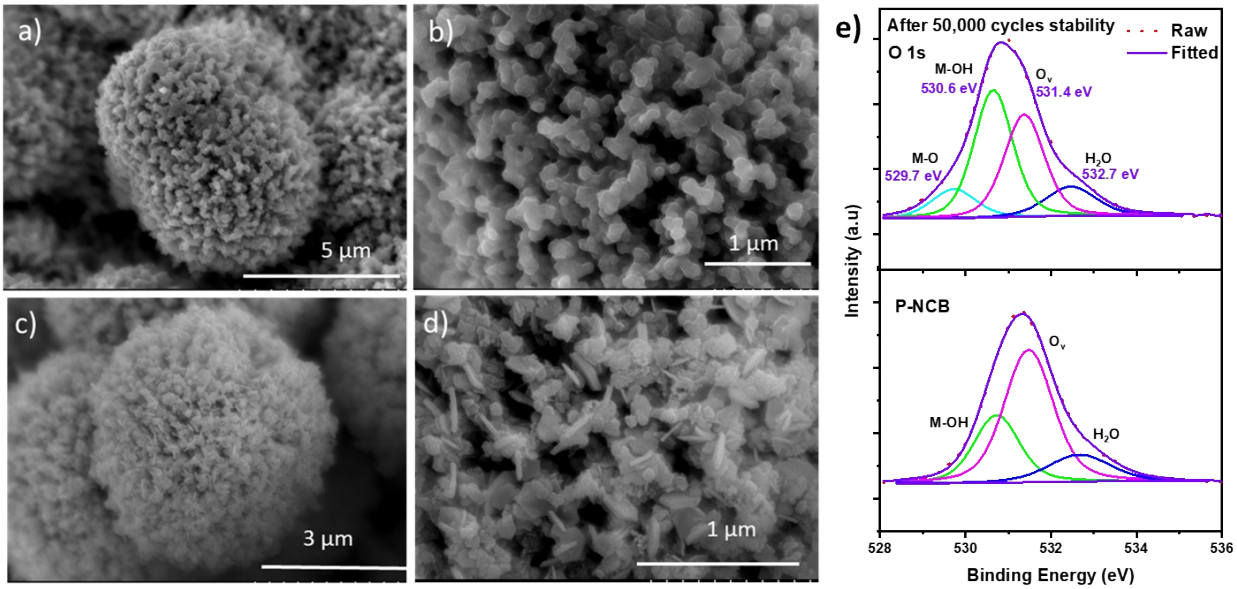

Fig. S7. SEM images of (a, b) P-NCB and (c, d) post 50,000 cycles of GCD stability sample e) XPS spectra of O 1s to indicate the O_v before and after 50,000 cycles stability.

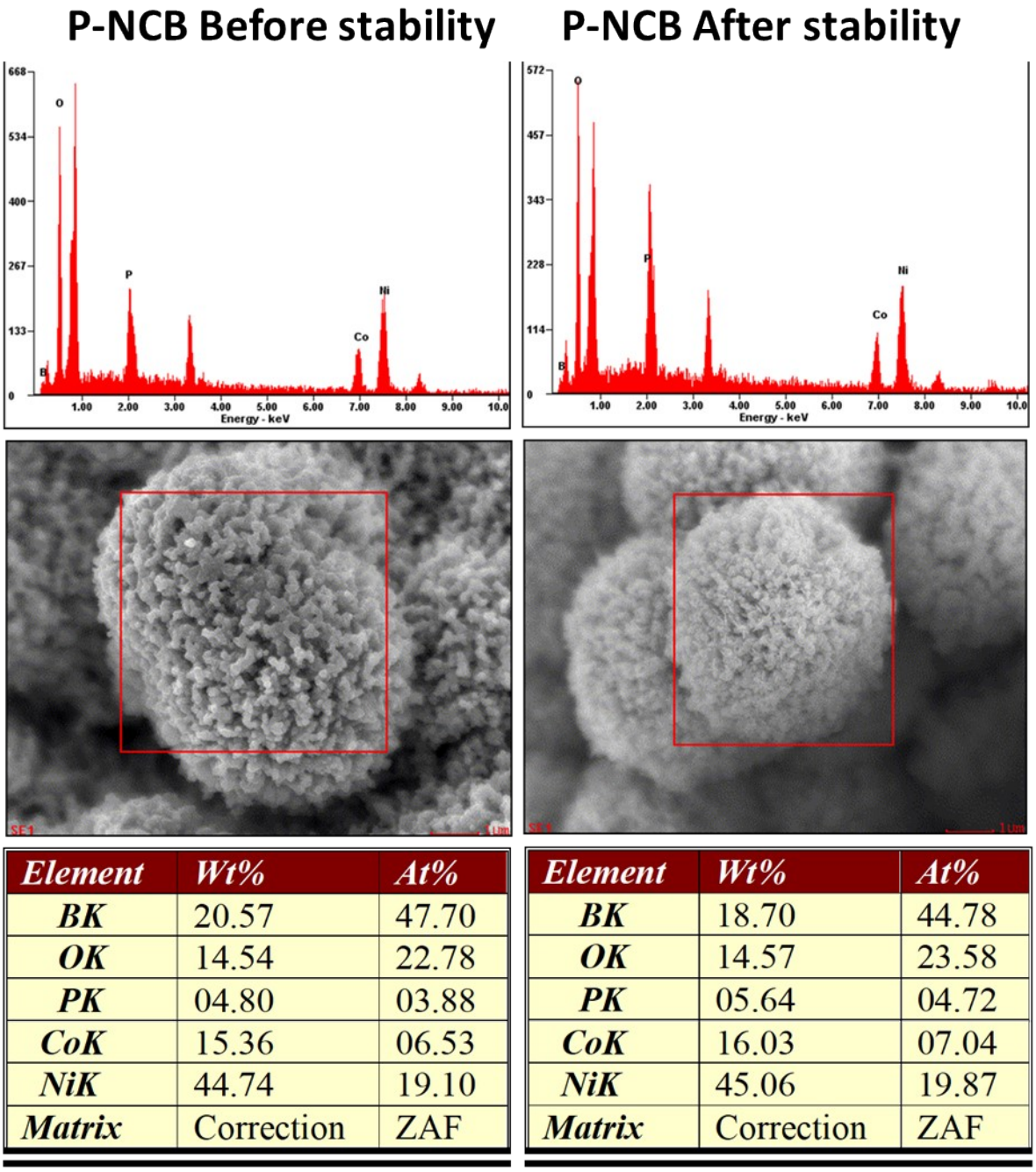

Element	Wt%	At%
BK	20.57	47.70
OK	14.54	22.78
PK	04.80	03.88
CoK	15.36	06.53
NiK	44.74	19.10
Matrix	Correction	ZAF

Element	Wt%	At%
BK	18.70	44.78
OK	14.57	23.58
PK	05.64	04.72
CoK	16.03	07.04
NiK	45.06	19.87
Matrix	Correction	ZAF

Fig. S8. EDAX analysis on elemental composition of P-NCB (a) before stability and (b) after 50,000 cycles of GCD stability sample.

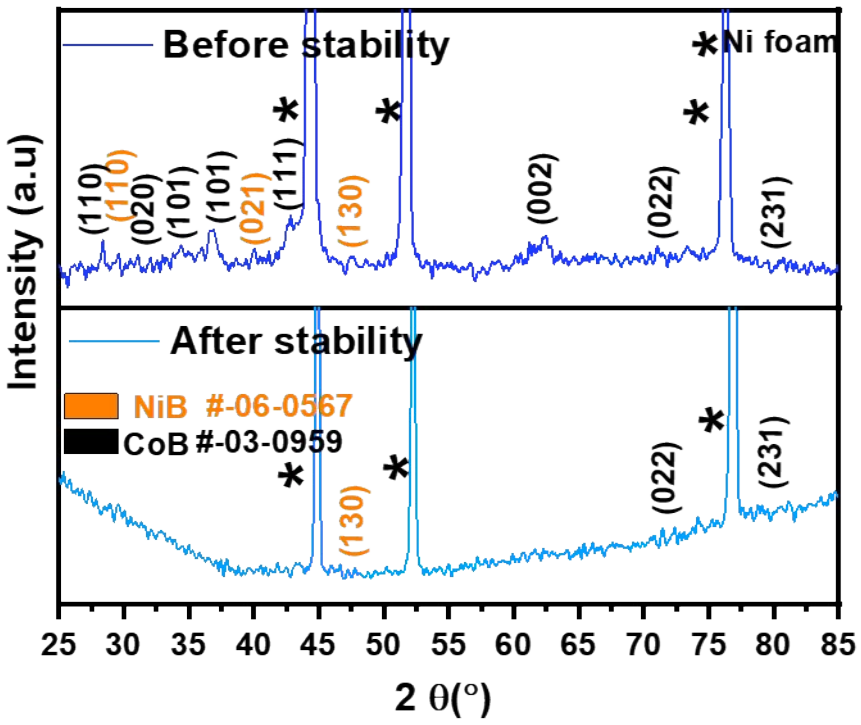

Fig. S9. XRD images of P-NCB pre and post 50,000 cycles of GCD stability sample

Trasatti Method

The contributions of the pseudocapacitive and electrical double layer mechanisms are typically calculated using the Trasatti method[3, 4]. First, the areas of the CV curves at various scan rates are evaluated and the capacitance is calculated using the following formula:

$$C = \frac{A}{2\,\Delta V\,v}$$

where C is the areal capacitance (mF/cm^2), ΔV refers to the potential window (V), and A is the area enclosed by the CV curves (mAV/cm^2) at different scan rates v (V/s). Assuming a semi-infinite diffusion pattern of ion diffusion, a linear relationship can be derived between the reciprocal of areal capacitance ($1/C$) and square root of scan rates ($v^{1/2}$) as follows:

$$\frac{1}{C} = \frac{1}{C_T} + cv^{1/2}$$

where C_T is the maximum capacitance (mF/cm^2), the sum of the contributions of the pseudocapacitive and electrical double layer mechanisms, and c is a constant. The electrical double layer contribution can be calculated using the following relation,

$$C = C_{EDLC} + cv^{-1/2}$$

The intercept obtained from linear fitting of the above relationship gives the value of the electrical double layer contribution at the maximum areal capacitance. The subtraction of C_{EDLC} from C_T yields the maximum pseudocapacitance (C_D).

$$C_D = C_T - C_{EDLC}$$

The power-law equation was employed

$$i = av^b$$

$$\log i = \log a + b \log v$$

where i is the redox peak current (mA), v is the scan rate (mV/s), and a and b are constants[5].

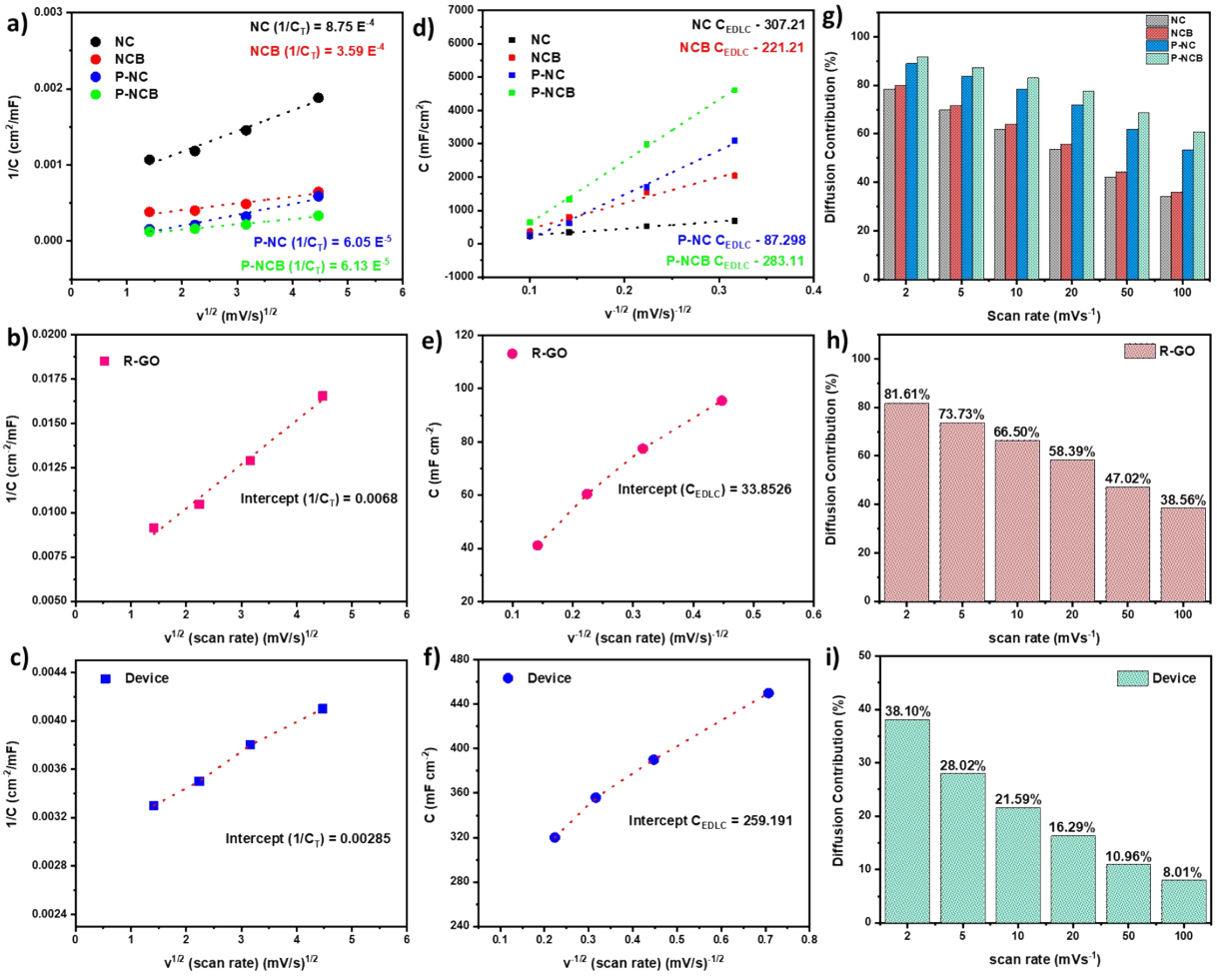

Fig. S10. (a, b, c) Plots of reciprocal of areal capacitance (1/*C*) versus square root of scan rates ($v^{1/2}$) and (d, e, f) plots of gravimetric capacitance (*C*) versus reciprocal of square root of scan rate ($v^{-1/2}$) and (g, h, i) Calculated contribution of diffusion controlled charge storage mechanism of the P-NCB, R-GO and device P-NCB//R-GO respectively.

Calculation of Surface-Active Sites

Associated charge with the reduction peak (Q) can be calculated using the following expression[6]:

$$Q = \frac{\int I \, dV}{v}$$

where Q (C) is the total charge associated with the reduction peak and v (V/s) is the scan rate. For simplicity, we assume that all the surface redox reactions are single electron transfer reactions. Then, the number of electrons calculated above is the number of surface-active sites (N). q = 1.602 $\times 10^{-19}$ C.

$$N = \frac{Q}{q}$$

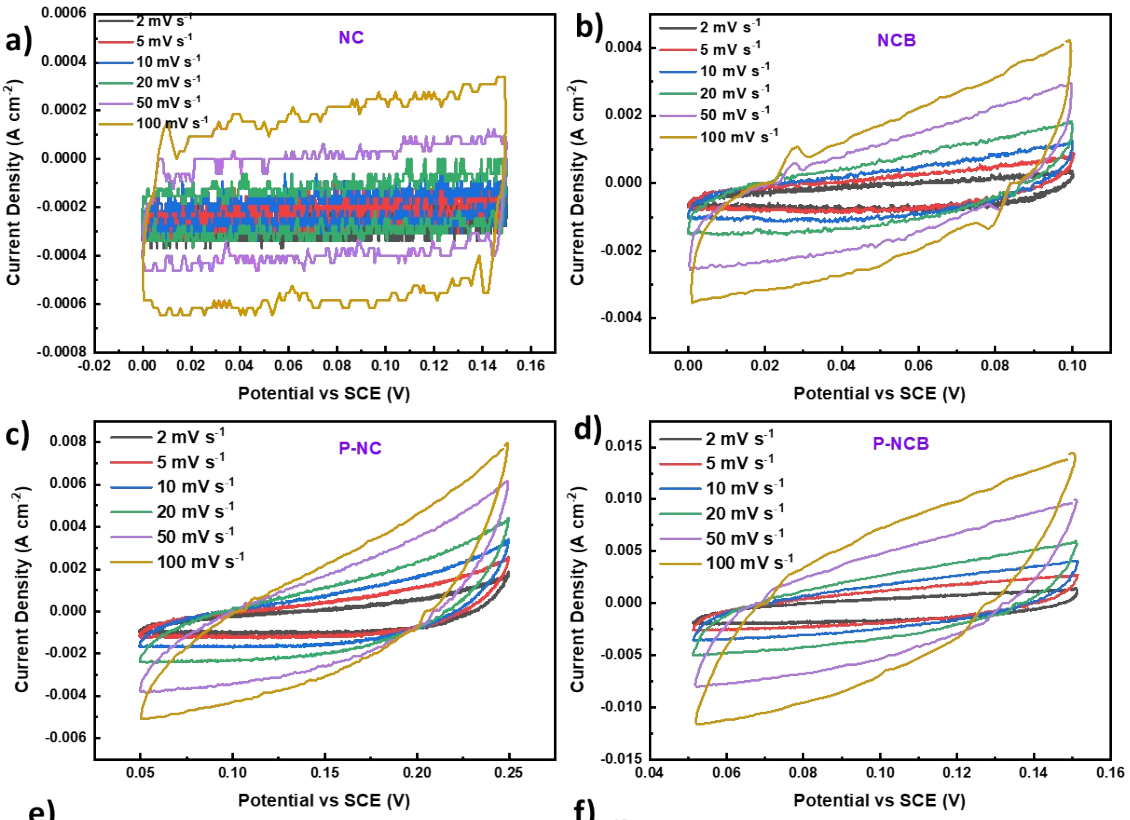

e)

Electro-catalyst	C_{dl} (mF cm^{-2})	ECSA (cm^2)
NC	3.73	93.25
NCB	16.55	413.75
P-NC	20.13	503.25
P-NCB	59.64	1491

Fig. S11. CV profile of non-faradaic regions of (a) NC, (b) NCB, (c) P-NC, (d) P-NCB respectively, (e) ECSA calculation derived from C_{dl}, and (f) Nyquist plots for the as-prepared samples at 0.4 V_{SCE} and the image shows the electrochemical equivalent circuit (inset: magnified image of Nquist plot).

Table S1. A comparison between the solution resistance (Rs) and charge transfer resistance (Rct) of the samples after fitting the EIS data.

Sample	R_s (Ω cm^{-2})	R_{ct} (Ω cm^{-2})
NC	1.593	10.51
NCB	1.606	1.4945
P-NC	1.601	1.608
P-NCB	1.592	0.409

Table S2. Comparison of the electrochemical performance in 2 M KOH solution of the P-NCB in three electrode setup with reported electrocatalysts.

S. No.	Material	Electrolyte	Specific capacitance, F/g, or Capacity, C/g (Current density, A/g)	Stability (Cycles)	Ref.
1	P-NCB	2 M KOH	3502 F/g or 1576 C/g (2 A/g)	85.20% (50,000) @ 40 A/g	This work
2	Ni-Co-B	6 M KOH	2226.96 F/g (1 A/g)	94.9% (1,000) @ 5 A/g	7
3	NCB@NCB_i	2 M KOH	2415 F/g (1 A/g)	91.2% (5,000) @ 5 A/g	8
4	Ni_xB/G	6 M KOH	1822 F/g (1 mV/s)	96% (2,000) @ 3 A/g	9
5	PMNC/G-*x*	6 M KOH	1668 F/g (0.5 A/g)	83% (2,000) @ 3 A/g	10
6	CoB–AC	6 M KOH	412 F/g (1 A/g)	66.7% (10,000) @ 5 A/g	11

7	$Ni_3V_2O_8$@Co-B	6 M KOH	216 mAh/g (500 mA/g)	NA	12
8	NiCoP	1 M KOH	1691 F/g (1 A/g)	80% (10,000) @ 10 A/g	13
9	NiB	2 M KOH	2230 F/g (1 A/g)	97.9 % (2,000) @ 10 A/g	14
10	NCP-4	1 M KOH	2228 F/g (1.5 A/g)	85 % (5,000) @15 A/g	15

141

142 **Table S3.** Comparison of the electrochemical performance of device prepared using P-NCB// R-GO

143 with reported other device setups.

S. No.	Supercapacitor/Supercapattery devices	Cell voltage (V)	Electrolyte	C_s (F/g) (Current density, A/g)	Stability (Cycles)	Energy density (Wh/kg)	Power density (W/kg)	Ref.
1	**P-NCB//R-GO**	**1.5**	**2 M KOH**	**202 F/g (303 C/g) (2 A/g)**	**83.33% (15,000) @ 15 A/g**	**63/41**	**750/15k**	**This work**
2	NCB-2//AC	1.6	2 M KOH	191.2 F/g (1 A/g)	93.8% (5,000) @ 2 A/g	74/24	420/18k	8
3	Ni_xB/G//activated carbon	1.6	6 M KOH	133 F/g (1 A/g)	96% (2,000) @ 5 A/g	50/22	200/2.5k	9
4	PMNC/G-2//AC	1.4	2 M KOH	122 F/g (5 A/g)	83% (10,000) @ 5 A/g	41/29	216/4.2k	10
5	CoB–AC//AC	1.6	6 M KOH	53.8 F/g (0.25 A/g)	80 % (10,000) @ 2 A/g	19/8	200/8k	11
6	$Ni_3V_2O_8$@Co-B//AC	1.6	6 M KOH	257 F/g (500 mA/g)	47 % (10,000)	91/21	400/8k	12

					@ 5 A/g			
7	NiCoP//AC	1.4	1 M KOH	256.2 F/g (2 A/g)	NA	36/29	1.8k/8.3k	[13]
8	NiB//AC	1.6	2 M KOH	135.5 F/g (1 A/g)	88.2 % (5,000) @ 5 A/g	59/8.7	1k/13.5k	[14]
9	NCP-4//AC	1.6	1 M KOH	90 F/g (0.4 A/g)	89 % (4,000) @ 5 A/g	32/23.1	320/1.6k	[15]

References

1. T. Kavinkumar, A. T. Sivagurunathan and D.-H. Kim, *Appl. Surf. Sci.*, 2023, **616**, 156453.
2. S. Adhikari, S. Selvaraj, S.-H. Ji and D.-H. Kim, *Small*, 2020, **16**, 2005414.
3. Z. Chen, V. Augustyn, X. Jia, Q. Xiao, B. Dunn and Y. Lu, *ACS Nano*, 2012, **6**, 4319-4327.
4. S. Ardizzone, G. Fregonara and S. Trasatti, *Electrochim. Acta.*, 1990, **35**, 263-267.
5. X. Yin, C. Zhi, W. Sun, L.-P. Lv and Y. Wang, *J. Mater. Chem. A*, 2019, **7**, 7800-7814.
6. S. Seenivasan, H. Jung, J. W. Han and D.-H. Kim, *Small Methods*, 2022, **6**, 2101308.
7. R. Chen, L. Liu, J. Zhou, L. Hou and F. Gao, *J. Power Sources.*, 2017, **341**, 75-82.
8. Q. Zhang, J. Zhao, Y. Wu, J. Li, H. Jin, S. Zhao, L. Chai, Y. Wang, Y. Lei and S. Wang, *Small*, 2020, **16**, 2003342.
9. Y. Chen, T. Zhou, L. Li, W. K. Pang, X. He, Y.-N. Liu and Z. Guo, *ACS Nano*, 2019, **13**, 9376-9385.
10. Y. Chen, W. K. Pang, H. Bai, T. Zhou, Y. Liu, S. Li and Z. Guo, *Nano Lett.*, 2017, **17**, 429-436.
11. J.-F. Hou, J.-F. Gao and L.-B. Kong, *New J. Chem.*, 2019, **43**, 14475-14484.
12. J.-F. Hou, J.-F. Gao and L.-B. Kong, *Electrochim. Acta.*, 2021, **377**, 138086.

13. M. Gao, W.-K. Wang, X. Zhang, J. Jiang and H.-Q. Yu, *J. Phys. Chem. C.*, 2018, **122**, 25174-25182.

14. W. Li, S. Wang, M. Wu, X. Wang, Y. Long and X. Lou, *New J. Chem.*, 2017, **41**, 7302-7311.

15. S. J. Marje, S. S. Pujari, S. A. Khalate, V. V. Patil, V. G. Parale, T. Kim, H.-H. Park, J. L. Gunjakar, C. D. Lokhande and U. M. Patil, *J. Mater. Chem. A.*, 2022, **10**, 11225-11237.